Journal of The Electrochemical Society

The Electrochemical Society
Advancing solid state & electrochemical science & technology

OPEN ACCESS

On the Role of Trigger Signal Spreading Velocity for Efficient Self-Healing Coatings for Corrosion Protection

To cite this article: Matthias Uebel *et al* 2018 *J. Electrochem. Soc.* **165** C1017

On the Role of Trigger Signal Spreading Velocity for Efficient Self-Healing Coatings for Corrosion Protection

Matthias Uebel,[1] Loïc Exbrayat,[2] Martin Rabe,[1] The Hai Tran,[1] Daniel Crespy,[2,3] and Michael Rohwerder[1,*,z]

[1]*Max-Planck-Institut für Eisenforschung GmbH, 40237 Düsseldorf, Germany*
[2]*Max-Planck-Institut für Polymerforschung, 55128 Mainz, Germany*
[3]*Department of Materials Science and Engineering, School of Molecular Science and Engineering, Vidvasirimedhi Institute of Science and Technology, Rayong 21210, Thailand*

Smart self-healing coatings for corrosion protection safely store active substances which are only released when corrosion occurs. This type of case-sensitive release has to be triggered by parameters that change as a consequence of corrosion. Examples are a change of pH, ionic strength, and electrochemical potential. In most technically relevant applications, a global release of active substances is not possible, i.e. the spreading of the signal which triggers the release of active substances is restricted to a lateral transport through the coating. Hence, the ability of the trigger signal to spread quickly through the coating from the local corroding area is crucial to create highly responsive and effective self–healing coatings. Here we show how the velocity at which the trigger signal spreads laterally along the metal|coating interface can be accelerated and how a penetration of the signal vertically into the coating, i.e. far away from the metal|coating interface, can be achieved.
 [DOI: 10.1149/2.0811816jes]

Manuscript submitted October 16, 2018; revised manuscript received December 7, 2018. Published December 19, 2018. This was Paper 771 presented at the National Harbor, Maryland Meeting of the Society, October 1–5, 2017.

Preventing corrosion of metals is of significant importance for many industries, such as automotive, appliances, aerospace or construction, and is associated with safety, economic and ecological issues.[1] The global cost of corrosion in 2013 was approx. 2.02 trillion € (~2.5 trillion US$), which is ~3.4% of the global gross domestic product.[2]

The protection provided by current industrial coatings is still based on technical developments dating far back into the 20th century.[3] The prevailing strategy in the coatings industry is to create coatings that are as delamination resistant as possible. Usually, active pigments that leach inhibitors upon the uptake of water are added to the coatings to further increase the corrosion resistance. However, most inhibitors are chemically active. An uncontrolled release of active substances poses a serious ecological problem and can also endanger the public health after prolonged exposure times. This has led to a legal ban on the use of hazardous corrosion inhibitors, such as chromates, in many industrial sectors.[4,5] Most likely the number of restricted inhibitors will expand in the future and might also include inhibitors that are currently still in use.[6] Therefore, new concepts or improved strategies for corrosion protection are urgently needed.

Smart self-healing coatings are a feasible way to overcome the mentioned drawbacks.[7–9] The challenge here is the safe long-term storage of healing agents, such as inhibitors or monomers and catalysts, within the coating and to ensure their sufficient release in case of a damage event. Various delivery systems for self-healing coatings have been reported and recently reviewed in literature.[10] The most suitable system may depend on the specific application and the relevant environmental conditions and in some cases combining complementary approaches might be favorable.

For many practical relevant applications, metallic components are exposed to atmospheric corrosion conditions and require strong barrier type topcoats. A global activation of the coating and transport of the released inhibitors via the bulk electrolyte is then not possible.

If under these conditions a penetrative coating defect arises, for instance by a scratch, the barrier function is locally lost, and corrosion could set in at this defect site. In that case, the release and transport of inhibitors has to occur laterally through the coating, and an immediate and strong response of the surrounding coating is required to stop corrosion. The self-healing performance is in general directly linked to the amount of active substances released and transported to the damaged area. Hence, in the stated scenario the velocity at which the trigger signal spreads through the coating is a crucial parameter. It is proposed here, that self–healing (SH) coatings which enable a fast spreading of the trigger signal will feature superior healing performance, especially in the presence of larger defects, as compared to delamination resistant SH coatings with a slower velocity of trigger signal spreading (Figure 1).

The highly challenging conditions often experienced in technically relevant applications are often neglected in studies reporting on self-healing coatings. Here, we present a counter–intuitive concept that targets on increasing the velocity at which the trigger signal spreads laterally and vertically through the coating.

Trigger signals related to corrosion and their ability to spread through the coating.—Recently, possible trigger signals exclusively related to corrosion were reviewed and discussed.[11] Here we focus on their ability to spread through the coating.

The trigger signal that is probably the easiest to implement and which is widely investigated is mechanical damage.[7,12,13] In fact, it is not a consequence of corrosion, but often initiates it. However, this trigger signal will not spread into the coating as it will only lead to opening of inhibitor loaded containers at the edges of the defect. Besides that, mechanical damage may not always result in corrosion, e.g. if the defect is not completely penetrating the coating to the metal surface. Furthermore, corrosion may also start without a mechanical impact, e.g. at weak and contaminated sites at the metal|coating interface, i.e. this trigger signal is not sensitive for corrosion induced by other mechanisms.

The local change of the pH value conditioned by local corrosion processes represents a prevailing trigger signal which is more advantageous. Usually, the pH will increase at the delaminating metal|coating interface, because OH^- ions are formed during the partial cathodic reaction, the oxygen reduction reaction.[14] The release of inhibitors upon changes of the pH value can be achieved by different mechanisms, such as structural changes of polyelectrolytes[15–17] or conducting polymers,[18] ion-exchange reactions,[19] e.g. by the use of Layered Double Hydroxides (LDH),[20–22] and pH dependent solubility of inhibitor pigments[23,24] or the container material itself.[25,26] However, for all pH triggered systems, the lateral spreading velocity along the

*Electrochemical Society Member.
zE-mail: rohwerder@mpie.de

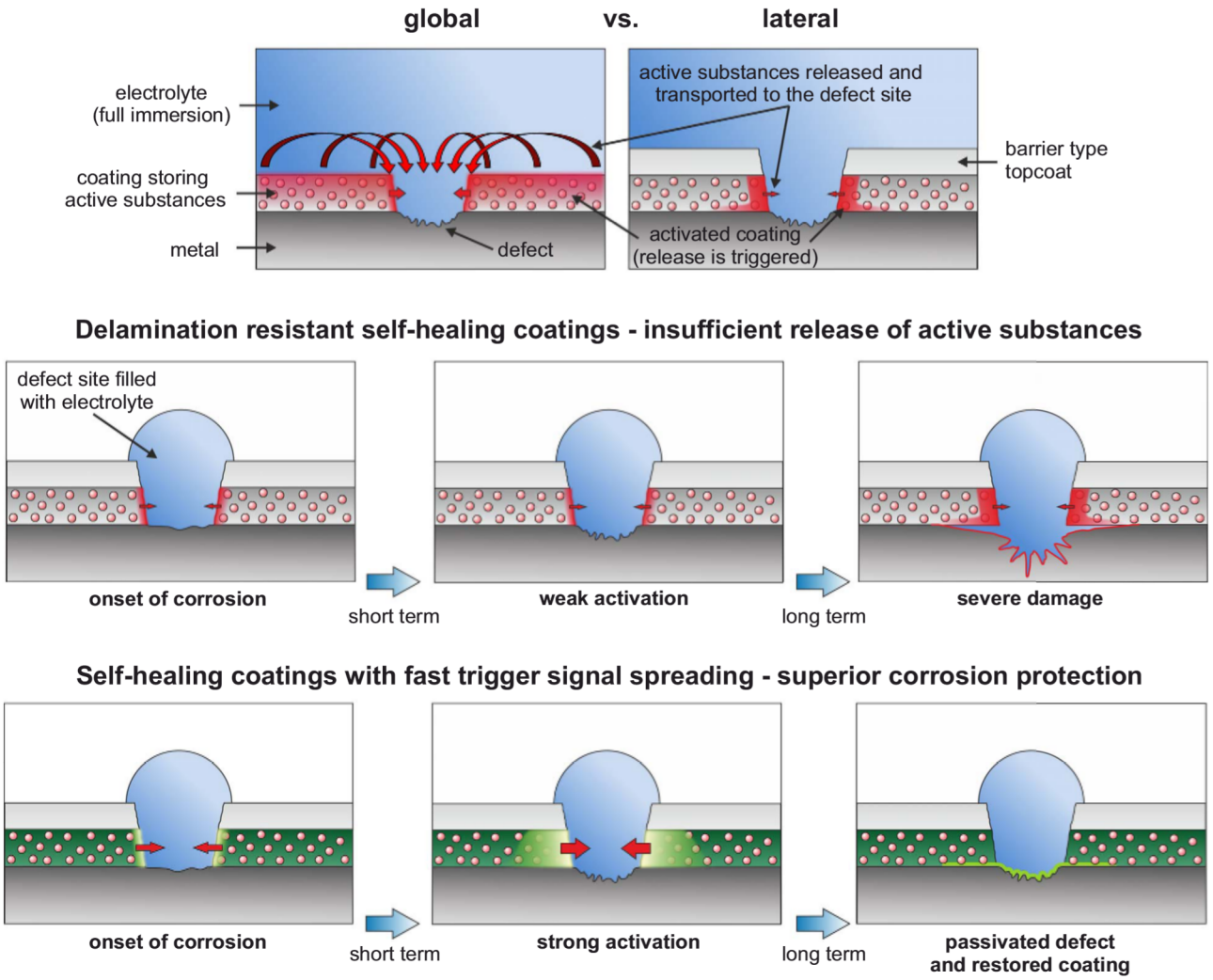

Figure 1. A global activation of self-healing coatings via the bulk electrolyte can trigger a huge release of active substances quite easily. However, the signal which triggers the release of active substances has to spread through the coating (even under full electrolyte immersion conditions), if barrier type topcoats are applied (upper row). Then the velocity at which the trigger signal spreads becomes the crucial factor: Delamination resistant self-healing coatings weakly trigger the release of active substances, which might be insufficient for self-healing of corrosion (middle row). On the contrary, a rapid trigger signal spreading velocity can enable sufficient release of active substances leading to self-healing of corrosion (lower row).

metal|coating interface is limited, and the extent of vertical propagation into the coating is questionable (especially when hydrophobic coatings are used). One possibility to direct the propagation of the change in the pH value more far away from the metal|coating interface, may be achieved by a suitable release system, e.g. by transport facilitating channels provided by hollow fibers containing pH responsive containers.[27] However, the magnitude of change in the pH strongly depends on the environmental conditions and the type of metal, and often the applied release mechanisms are irreversible.[28–30] Even if the applied release mechanism is reversible, it is still not switched completely case-sensitively (intelligent release) since the release will only stop when the pH value has dropped sufficiently again, but corrosion might have stopped much earlier.

Therefore, the by far most reliable and case sensitive trigger signal related to corrosion is the change in electrochemical potential for the following reasons: the electrochemical potential will only decrease significantly as compared to the passive metal|coating interface's potential upon onset of corrosion. As soon as the corrosion is stopped, the electrochemical potential will change accordingly. In that way an immediate switching of release or safe storage of inhibitors is possible. This fact is independent of the type of metal, coating and the environmental conditions.[11] The most important aspect, however, is that the change in electrochemical potential probably represents the only trigger signal for which the velocity of spreading (laterally as well as vertically within the coating) can be specifically adjusted.

Background and approach of this work.—In this study (nano-)capsules are used, which consist of an intrinsically conducting polymer (PolyAniline, PAni) shell with the organic corrosion inhibitor (3-nitrosalicylic acid, 3-NisA) safely stored inside a hydrophobic solvent core,[31] here denoted as PAni(3-NisA) capsules.

The mechanism by which 3-NisA is released from the PAni capsule is based on the capsules shell (thickness $\sim$ 50 nm), which becomes permeable upon electrochemical reduction.

Positive charges within the polymer backbone are present when PAni is in its oxidized state and these are counterbalanced by dodecyl sulfate anions (DS^-). Upon electrochemical reduction of PAni, small cations (K^+) will be incorporated within the PAni capsules shell (Figure 2). The hydrophilicity increases and uptake of water leads to a swelling of the PAni shell.[32] The PAni capsules shell becomes porous, creating at some points water|oil interfaces which connect the hydrophobic core of the PAni capsule with the surrounding aqueous electrolyte. The concentration gradient of corrosion inhibitor at the created oil|water interface drives a diffusion assisted release of the corrosion inhibitor from the PAni capsules.

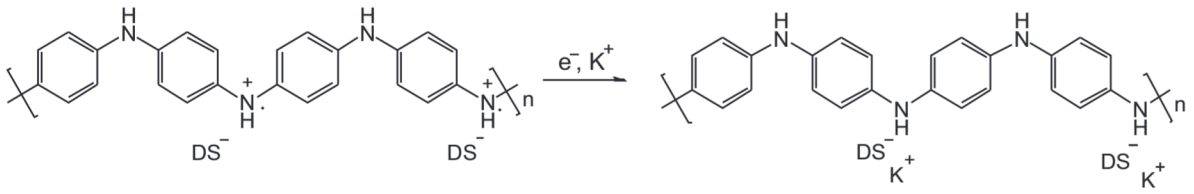

Figure 2. Reaction scheme of the electrochemical reduction of polyaniline (PAni) (adapted from Ref. 35). The oxidized groups within the polymer backbone are counterbalanced with dodecyl sulfate anions (DS^-). The reaction scheme shows the incorporation of small cations upon reduction of PAni for charge compensation.

The release was quantified and proven to be reversible and a successful self-healing of a defect inflicted to an organic coating on zinc was demonstrated.[31,33] In the afore–mentioned work, the PAni(3-NisA) capsules needed to be modified with conducting spacer particles (for ease of preparation here gold nanoparticles (AuNPs) were used) to prevent the formation of an insulating layer at the zinc|capsules interface.[33] This effect is usually observed when chemically synthesized Intrinsically Conducting Polymer (ICP) is applied directly onto zinc (more detailed discussions can be found in the literature[34] and below) and it would hinder the capsule's permeability from being switched on or off, here denoted as addressability.

However, the release rate of inhibitors from the PAni(3-NisA) capsules directly applied onto zinc is limited for two reasons: first, the lateral trigger signal spreading velocity is limited by the delamination rate, and secondly only the PAni(3-NisA) capsules in direct contact with the metal substrate can be electrochemically reduced, thus only a limited release of inhibitors can be triggered.[35]

Here we demonstrate that the trigger signal spreading velocity can be accelerated by introducing an intermediate layer of ICP (PolyPyrrole, PPy) between the metal and PAni(3-NisA) capsules. This results in an increased release of active substances leading to enhanced passivation by ~100% as compared to a reference system due to faster lateral spreading of the trigger signal. Furthermore, a restoration of the activated coating after passivation of the defect site is achieved, and the coating provides an increased interfacial stability with inherent self-healing ability of very small defects,[36] such as pinholes, without the need of inhibitor release from PAni(3-NisA) capsules. It will also be shown that the spreading velocity of the electrochemical potential indeed can be specifically adjusted, and that this affects the amount of released substances. Finally, embedding of PAni(3-NisA) within PPy overcomes the limitation of vertical addressable capsules.

The mechanism by which PAni capsules release corrosion inhibitors and the approach of this work (and our previous work)[33] are schematically summarized in Figure 3: The electrochemical reduction or re-oxidation of the PAni capsules shell, which will be accompanied by the uptake or expulsion of small cations (K^+), allows an immediate switching between release or safe storage of corrosion inhibitors, respectively (Figure 3a). The release of inhibitors from the PAni(3-NisA) capsules as part of a coating is directly linked to the delamination rate, as the coating delamination is associated with a decrease of the electrode potential in the delaminated region. The drop of the electrode potential followed by a thin electrolyte layer penetrating the delaminated interface leads to the electrochemical reduction of PAni(3-NisA) capsules. Hence, the coating delamination rate represents the lateral trigger signal spreading velocity, which is fixed to a certain value according to the delamination kinetics of the metal|coating interface (Figure 3b). The concept of this work is to accelerate the reduction rate of PAni capsules and the associated release of inhibitors by the introduction of a continuous layer of polypyrrole between the metal and the PAni(3-NisA) capsules, which accelerates the mobility of small cations (Figure 3c). Finally, the vertical addressability of the PAni(3-NisA) capsules can be improved by embedding into PPy (Figure 3d).

We prove the proposed concept by demonstrating (multiple) self-healing of macroscopic defects within an organic coating applied on zinc (a model system for galvanized steel that is widely used).

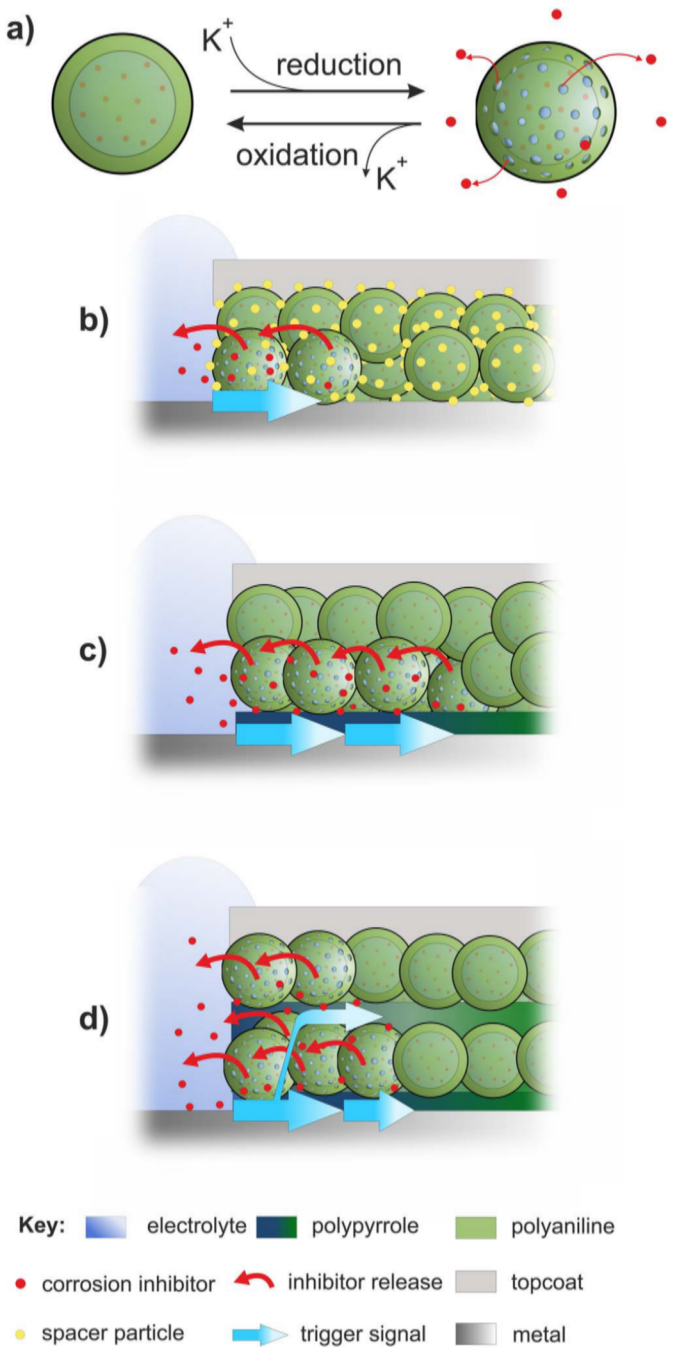

Figure 3. a) Schematic illustration of the mechanism by which capsules release corrosion inhibitor. Trigger signal spreading and the associated release of inhibitors for b) capsules directly applied onto the metal (note, in this case capsules have to be decorated with conducting spacer particles),[33] c) with interlayer of conducting polymer (polypyrrole), d) with capsules additionally embedded within polypyrrole.

Our findings are proposed to have general validity for self–healing materials based on triggered release of active substances.

Experimental

Materials and chemicals.—Zinc foils (thickness 1.5 mm, purity 99.95%) were purchased from Goodfellow. Potassium chloride (KCl), sodium hydroxide (NaOH), potassium hydroxide (KOH), ethanol (EtOH) and Poly (vinyl butyral-co-vinyl alcohol-co- vinyl acetate) (PVB) (MW $\approx$ 50 000–80 000 g mol^{-1}) were purchased from Sigma–Aldrich in p.a. quality and used without further purification. 3–nitrosalicylic acid (used without further purification) and pyrrole were purchased from TCI. Pyrrole was distilled twice under nitrogen before use. Water used for preparation of solutions was taken from USF ELGA water purification system (conductivity $\sigma < 0.055$ µS cm^{-1}).

For the synthesis of polyaniline capsules, ammonium peroxydisulfate (APS, analytical grade), sodium dodecyl sulfate (SDS, p.a.), 3-nitrosalicylic acid (3-NisA, $\gtrsim$ 99%,) were purchased from Sigma Aldrich and used without further purification. Polyvinyl alcohol (PVA, ~98%) was purchased from Alfa Aesar, and ethylbenzene (EB, p.a.) from ACROS Organics, both used without further purification. Aniline was purchased from Sigma Aldrich and distilled under vacuum prior use. Hydrogen tetrachloroaurate(III)trihydrate ($HAuCl_4 \cdot 3H_2O$, 99.99%) and trisodium citrate ($C_6H_5Na_3O_7$, 99%) were purchased from Alfa Aesar and used as received.

Synthesis, characterization and application of polyaniline capsules.—The synthesis of PolyAniline (PAni) capsules (with and without encapsulated corrosion inhibitor 3-nitrosalicylic acid), synthesis of gold (Au) NanoParticles (NPs), and the decoration of PAni capsules with AuNPs were carried out according to the mini–emulsion technique described elsewhere.[31,33] In brief, as dispersed phase 0.5 ml aniline, 1.2 ml ethylbenzene and 48 mg 3–nitrosalicylic acid are mixed by stirring at 1000 rpm for 15 minutes. The dispersed phase was dropped into the continuous phase consisting of 62.5 mg sodium dodecyl sulfate and 6 g water and stirred at 1000 rpm for 1 h. Emulsification was initiated by ultrasonication of the ice–cooled mixture for 240 s at 90% amplitude using a Branson sonifier W450. After ultrasonication, a stabilizer solution consisting of polyvinyl alcohol dissolved in water was added while stirring the solution at 500 rpm for ca. 5 minutes. The stabilizer solution was prepared before by mixing 1.5 g PVA in 15 g water at 90°C while it was stirred at 500 rpm for approx. 2 h (until PVA was completely dissolved), followed by cooling down to room temperature. Then a solution consisting of 1.23 g ammonium peroxydisulfate and 2 g water was slowly added dropwise to the solution, which initiated polymerization at the interface of dispersed phase droplets and continuous phase. The color of the solution turned to dark green. The capsules were washed repeatedly with ultrapure water until the supernatant appeared clear and collected by centrifugation at 8000 rpm. The purified capsules were finally dispersed in ultrapure water to a solid content of ~2 wt-%. The content of encapsulated inhibitor was ~3.1 wt-%, which was dissolved in ethylbenzene in the core of the capsules. Inhibitor free capsules were prepared the same way, but without addition of 3-nitrosalicylic acid to the dispersed phase.

AuNPs were prepared by mixing 2.4 g hydrogen tetrachloroaurate(III)trihydrate in 0.6 l ultrapure water. The solution was stirred and heated until it started boiling and then quickly 60 ml of a 2.5 mM trisodium citrate solution was added. The change of color from yellow to deep red indicated the formation of nano–sized gold particles (d $\approx$ 13 nm). The solution was kept stirring while the solution cooled down to room temperature.

The PAni capsules were decorated with AuNPs by stirring PAni dispersion together with AuNPs at 600 rpm for ca. 12 hours. The weight ratio of PAni to AuNPs was ~7:1. During this procedure the AuNPs adsorbed onto PAni capsules as it was proven by TEM observations.

The morphology of the PAni(3-NisA) capsules was investigated with a Transmission Electron Microscope (TEM) (JEOL 1400) operated at an accelerating voltage of 120 kV. TEM samples were prepared by dropping the dispersion with capsules on a copper grid (300 square mesh) coated with a carbon layer. The average diameter of the capsules was 1237 ($\pm$ 689) nm, and the capsules shell is about 50 nm thick.

PAni capsules were deposited on the substrates (PPy or zinc) via drop–casting of 50 µl cm^{-2} if not stated otherwise from an aqueous dispersion and dried in an oven at 75°C until the solvent was evaporated. Then a hydrophobic topcoat (PVB) was applied.

Treatment of zinc substrates.—Zinc foils were cut to specimens with a dimension of 25 × 15 mm and ground to a P1000 finish using SiC paper (grinding direction parallel to short edge of the specimen), cleaned with a detergent solution using cotton wool, rinsed and sonicated with deionized water and EtOH, respectively, and dried under an air stream. Zinc samples were pretreated prior to polypyrrole (PPy) layer electro–polymerization in a 3 electrode set–up with platinum counter electrode by cycling 5 times from −1.1 V to −1.4 V vs Ag/AgCl(3 M KCl) in NaOH (0.25 M) with a scan rate of 10 mV/s using a Solartron Schlumberger 1286 potentiostat. This treatment increased the ZnO layer thickness by about 30 nm as measured by XPS sputter depth profiles before and after the pretreatment. The ZnO layer protects Zn against dissolution during the electro–polymerization process for which anodic potentials are applied to the Zn sample. This is particularly necessary when pyrrole is electro-deposited on zinc at a low current density (~ 1 mA/cm^2) at a correspondingly low deposition rate.

X-ray photoelectron spectroscopy (XPS) of pretreated zinc.—XPS sputter depth profiles were obtained for Zn samples prior and after the pretreatment using a Quantum 2000 from Physical Electronics Inc. XPS was performed at a takeoff angle of 45° with a pass energy of 23.5 eV, a monochromatic Al Kα1 source (1486.7 eV) operating at 15 kV and 25 W on a spot size of 100 µm by 100 µm upon a base pressure smaller than 5 × 10^{-9} mbar. The software CASA XPS was used for processing the data.

Electro–polymerization and characterization of polypyrrole coatings on zinc.—The electro–polymerization of PPy was realized galvanostatically with a current density of 1 mA cm^{-2} or 5 mA cm^{-2} in a 3 electrode setup with zinc used as working electrode, platinum as counter electrode and Ag/AgCl(3 M KCl) as reference (purchased from Metrohm GmbH). An area of 8 × 18 mm was exposed to the stirred aqueous electrolyte solution (~70 mL) consisting of 0.3 M pyrrole and 0.01 M 3-nitrosalicylic acid (pH = 2.5, adjusted with KOH). 3-nitrosalicylic acid was chosen as supporting electrolyte as 3-nitrosalicylate is an effective corrosion inhibitor for zinc and thus provides additional protection against dissolution of the zinc substrate during the anodic electro–polymerization process.[37] The samples were rinsed immediately after electro–polymerization with H_2O and EtOH and dried in a N_2 stream.

The solution used for electro-polymerization was prepared as follows: water was heated to 60°C and 3-nitrosalicylic acid (3-NisA) was added under stirring until it was completely dissolved. Then pyrrole was added dropwise, and the solution was stirred overnight. After cooling to room temperature, the pH was adjusted to 2.5 using KOH.

The relationship of the resulting thickness s to the passed charge Q was obtained by synthesizing 3 samples at 5 mA cm^{-2} current density for different times. It was proven that the s:Q ratio holds still true for applied current density of 1 mA cm^{-2}.

Cross–sections were prepared by using a Hitachi Ion Milling System E-3500 operated at an acceleration voltage of 6 kV, a discharge voltage of 4 kV and a discharge current of 400 µA. The morphology and thickness of PPy layers and the pretreated Zn were measured with a Field Emission Scanning Electron Microscope (FE-SEM) from ZEISS (Model LEO 1550 VP, GEMINI) operated predominantly at an acceleration voltage of 15 kV and a working distance of 6–9 mm using the software SmartSEM v5.06.

Self-healing samples with embedded PAni(3-NisA) capsules were prepared in the following sequence: Zn was prepared as described including the pretreatment procedure, followed by electrodeposition of ~1.2 µm PPy, drop casting of 30 µl/cm^2 PAni(3-NisA) capsules dispersion, electrodeposition of ~1 µm Ppy onto PAni(3-NisA) capsules, drop casting of 30 µl/cm^2 PAni(3-NisA) capsules, electrodeposition of ~1 µm Ppy onto PAni(3-NisA) capsules, drop casting of 70 µl/cm^2 PAni(3-NisA) caspules dispersion and application of PVB topcoat.

Preparation of PVB topcoats.—Poly (vinyl butyral-co-vinyl alcohol-co- vinyl acetate) (PVB) coatings were prepared by spin-coating from an ethanolic PVB solution using a spin-coater from Speciality Coating Systems (Model P6700). The samples were spin-coated 4 times with a 5 wt-% PVB solution at 2000 rpm for 20 s, dried in an oven at 75°C for approx. 5 minutes, and then spin-coated 3 times with a 10 wt-% PVB solution at 2000 rpm for 20 s, again followed by drying at 75°C for approx. 5 minutes.

Scanning Kelvin Probe (SKP) measurements.—An artificial defect was inflicted to the samples according to literature[33] directed parallel to the short edge of the sample using a razor blade. The defect dimension is approx. 2300 (± 500) µm × 170 (± 20) µm × 40 (± 10) µm (length/width/depth) as measured on 5 scratches with a confocal microscope and the software µsoft control. This scratch was filled with 7.5 µL of 1 M aqueous KCl solution. The electrode potential at the defect site and the potential of the surrounding coating was monitored in-situ with a commercial SKP system from KM Soft Control in an alternating fashion: first, the potential at the defect site was measured for 1 min. by positioning the SKP-tip centered over the electrolyte drop and then line scans were started close to the electrolyte droplet covering the scratch. For this purpose, the SKP-tip was scanned at a constant distance to the sample surface for a distance of 4–10 mm in a line normal to the scratch with a step size of 50 µm or 100 µm away from defect. The SKP was operated with a paraffin coated 100 µm Ni(80)/Cr(20) SKP-tip[38] with an oscillation frequency of 934 Hz. Prior to every experiment the SKP was calibrated against a Cu/Cu^{2+} reference electrode in air at ~93% relative humidity (RH). For Fermi level misalignment tests surface scans of 2 × 2 mm (x × y) with a step size of 200 µm in x- and y-direction were measured while the atmosphere was changed from dry air (RH<0.2%), to humid air (RH ~93%) and finally to humid N_2 (RH ~93%).

Processing of SKP data.—For calculation of the delamination rates, a distinct potential E_{del} was chosen manually in such a way that it intersects all potential-distance curves in the steepest region, the delamination front. For this purpose, a MATLAB program was developed that enables a quick graphical assessment of this procedure. The position values x_{del} corresponding to E_{del} for each potential-distance curve were determined by interpolation of the two data points closest to E_{del}. From the x_{del}-t plots the linear region was selected and fitted with a linear function to yield the delamination rate including its standard derivation.

Results and Discussion

Conception and implementation to produce highly responsive self-healing coatings restricted to lateral trigger-, release- and transport processes.—To release more inhibitors, PAni(3-NisA) capsules must be activated (reduced) at a faster rate. In principle, the defect site, serving as the net anode, galvanically couples with the delaminating interface, the net cathode.[39] The corresponding reduction rate of capsules applied directly onto the metal is thus directly linked to the delamination rate, which in turn is determined by the zinc|coating interface. To enhance the release of inhibitors, here a strategy is proposed that is counter-intuitive, namely the acceleration of the delamination (reduction) rate. This approach appears contrary to the prevailing opinion in the industry on how a corrosion protection coating should be designed. However, it will be shown that for self-healing coatings a fast delamination (reduction) rate, thus fast trigger signal spreading, can lead also to a superior corrosion resistance.

This is achieved by introducing a polypyrrole (PPy) layer between the underlying metal (zinc) and the PAni(3-NisA) capsules layer. The electro-polymerization process of PPy is performed in the galvanostatic polarization mode since it allows an accurate control of the Ppy layer thickness (Figure 4a). The charge Q ($= i \cdot t$) passed during electro-polymerization correlates with the resulting polypyrrole layer thickness s. The PPy layer thicknesses were directly measured in a cross-section of the samples (inset in Figure 4a). The s:Q ratio is seemingly unaffected by the current density as the PPy thickness electro-deposited at 1 mA/cm^2 (1.5 C/cm^2) matches the linear regression based on PPy electro-deposited at 5 mA/cm^2. However, the current efficiency for the electro-polymerization of polypyrrole onto (reactive) zinc substrate is expected to be below 100%, as the passed charge required for electro-deposition of 1 micron of PPy is significantly higher as reported for electro-deposition of ICP on inert substrates such as Au or Pt (~0.2–0.4 C/µm · cm^2).[40] This may also be related to the partial over-oxidation of PPy used in this study.

The electrochemical stability of the zinc|PPy interface, which is a crucial requirement for the electrochemical addressability of capsules in contact with PPy, was tested in gas exchange experiments performed

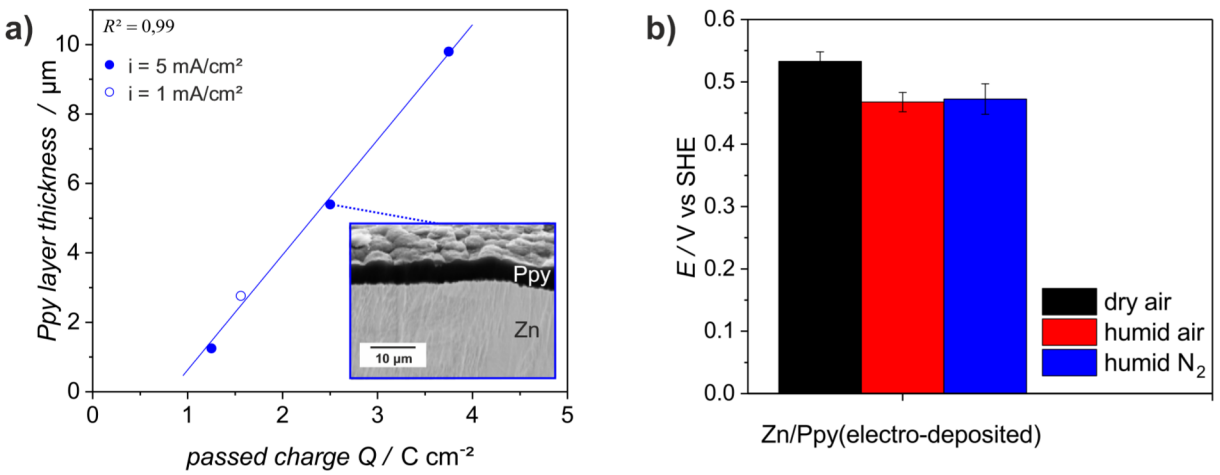

Figure 4. Synthesis and characterization of polypyrrole layers. a) Polypyrrole layer thickness as a function of passed charge (inset shows SEM image of PPy cross-section deposited for 2.5 C/cm^2). b) Qualitative study of the interfacial reactivity of Zn|PPy conducted with a Scanning Kelvin Probe (SKP) in gas exchange experiments: response of electrode potential upon varying atmosphere.

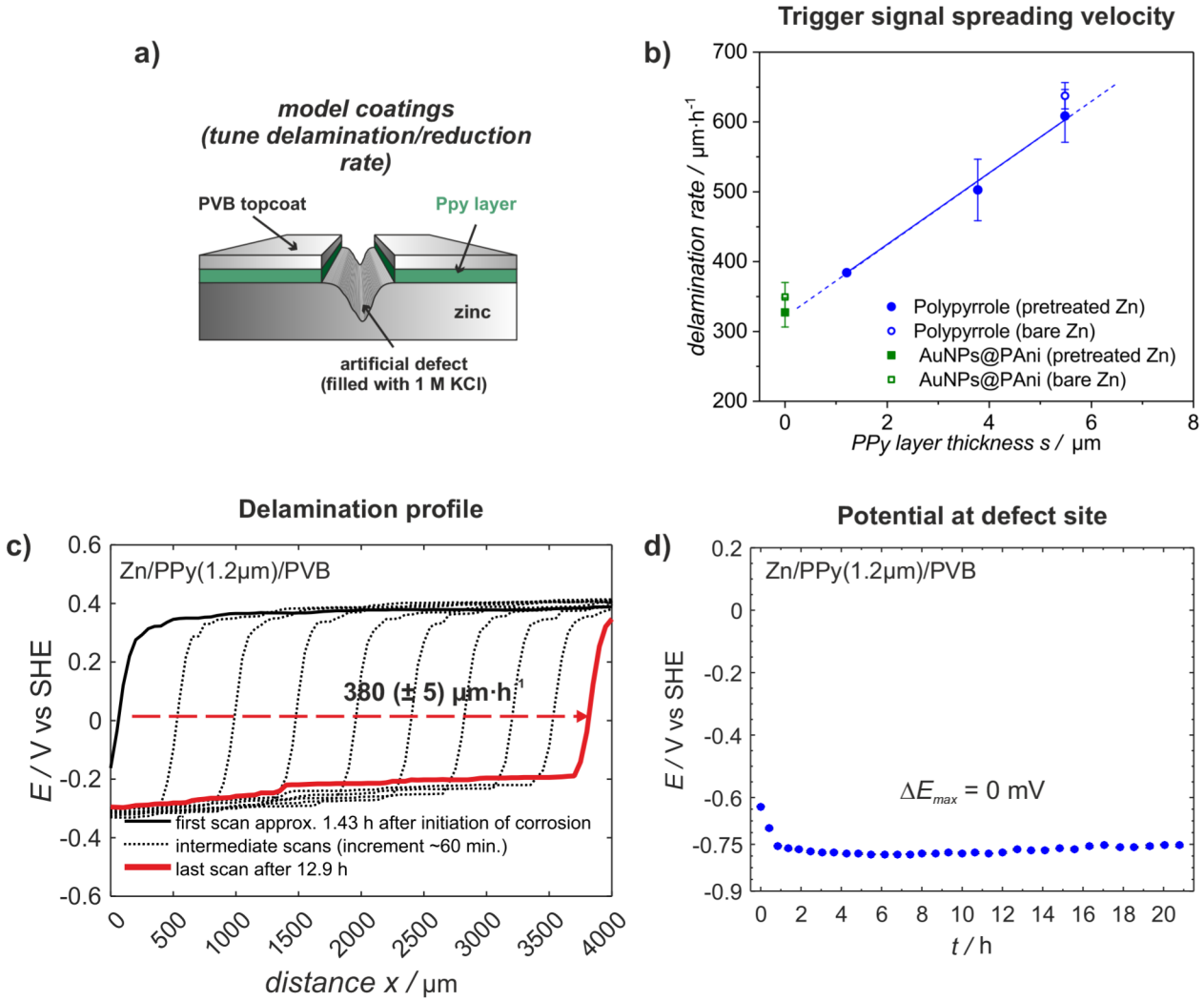

Figure 5. Accelerated lateral velocity at which the trigger signal spreads through the coating. a) Scheme of model coatings with hydrophobic topcoat. b) Trigger signal spreading velocity of the reference system (AuNPs@PAni) applied directly onto bare/pretreated zinc, and PPy electro-deposited with varying thickness onto bare/pretreated zinc. c) Delamination profile for polypyrrole (thickness = 1.2 µm) electro-deposited onto pretreated zinc and d) the corresponding electrode potential at the defect site.

with a SKP. During this test the atmosphere is changed from dry air to wet air and finally to wet nitrogen while the corresponding changes in the electrode potential are monitored, revealing the interfacial reactivity. Three different cases can be distinguished: active corrosion, Fermi level misalignment and a passive interface. An actively corroding system would show a clear potential difference upon transition from humid air to humid nitrogen.[34] For chemically synthesized ICP applied directly onto zinc, a significant potential difference would be detected upon switching the atmosphere from dry air to humid air, indicating the formation of an insulating interface accompanied by Fermi level misalignment.[34,41] In contrast, a passive interface can be observed for zinc|PPy(electrodeposited) as it is reflected by a quite constant potential during all three atmospheric conditions (dry air, humid air, humid nitrogen, Figure 4b). Obviously the active electro-polymerization process ensures the formation of a conductive and stable passive interface, as already observed in other works.[42] The high corrosion resistance at the interface is certainly also enhanced by the 3-NisA counter anions incorporated within the PPy, which are effective corrosion inhibitors for zinc.[37] This layer allows the application of capsules without the need to use conducting spacer particles, which was necessary in our previous work,[33] since the electronic coupling is now maintained via the zinc|PPy interface. Moreover, a protection against interfacial degradation due to radicals formed during the oxygen reduction reaction, an important key reaction during cathodic delamination,[43] is likely because of a possible shift of the oxygen reduction site beyond the zinc|PPy interface laterally into the coating.[36] Thus, the reduction of the conductive coating can be distinguished from the cathodic driven delamination of a non-conductive coating with respect to interfacial degradation. Furthermore, this protective PPy layer not only provides passive but also active protection, as it is also able to self-heal small defects in the passive metal oxide layer or pinholes within the coating.[36,44]

Relationship of trigger signal spreading velocity and self-healing performance.—Several model coatings were prepared and used for investigating the effect of different trigger signal spreading velocities as shown schematically in Figure 5a. Again, zinc is used as a substrate metal which is covered with electro-deposited polypyrrole.

Poly(vinyl butyral-*co*-vinyl alcohol-*co*- vinyl acetate) (PVB) is used as a hydrophobic topcoat. An artificial defect site is inflicted to this coating system and subsequently filled with an electrolyte solution (7.5 µl 1 M KCl) that initiates corrosion. Using the SKP technique, the time-dependent evolution of the electrode potential E at the defect site and the cathodic driven delamination progress were monitored in-situ under atmospheric corrosion conditions (for detailed information about the SKP technique and the realized type of experiments see previous publications).[45–48] In brief, the SKP-tip serves as a natural reference electrode for a contactless measurement of the electrode

potential of metals covered by a thin layer of electrolyte or a coating. This allows it to monitor the electrode potential at the defect site, which is a penetrative coating defect covered with a little droplet of electrolyte, by positioning the SKP-tip close over the surface of the electrolyte. By scanning the SKP-tip close over the coating in a line away from the defect site, the electrode potential at the metal|coating interface is measured as a function of distance to the defect site. The potential-distance curves can be distinguished into 3 regions: lower potentials represent the delaminated region, higher potentials represent the intact metal|coating interface, and the sharp increase in potential from the delaminated region to the intact one indicates the current position of the delamination front. Repetitive performed line scans yield the delamination profile, which reveals the time dependent evolution of the measured potential-distance curves. The progression of the delamination front for example represents the delamination rate.

Figure 5b summarizes the effect of PPy layer thickness and the pretreatment of Zn on the delamination rate. Note, at this point no inhibitor loaded PAni capsules are added to the coatings. It is observed for pretreated Zn coated with electro-deposited PPy, that the delamination rate increases with increasing PPy layer thickness. The reduction rate of PPy crucially depends on the transport of cations. With decreasing PPy layer thickness the mass transport of cations in the reduced ICP decreases. This was also found in the past for thin PPy layers ($< 1\mu m$).[51] While in N_2 atmosphere the reduction front proceeds for all PPy films independent of the thickness at the same rate, in air the ORR at the low potentials of the reduced PPy has to be enabled by sufficient cation flow. Thin PPy coatings cannot provide that, as the mass transport is proportional to the PPy film thickness. That retards the progress of the reduction front, because for thin coatings the delamination of interface has to occur first for providing sufficient cation transport also along the delaminated interface. For very thick coatings, the mass transport through the reduced PPy is sufficient and the reduction progress in air is similar to the one in N_2 atmosphere. Hence, in a certain thickness range the reduction progress will increase with the PPy layer thickness as it is presented here. Thus, the thickness of the PPy layer is an ideal parameter for investigating the interplay between trigger signal spreading velocity and self-healing performance: adjusting different thicknesses of PPy layers leads to different trigger signal spreading velocities (delamination rates), thus enhancing the release of inhibitors while the chemistry of the system remains the same. The kind of pretreatment of zinc shows only a slight effect on the delamination rate due to inhibition of the oxygen reduction reaction (ORR): the delamination rate decreases only by approx. 5% when zinc is pre-oxidized.

The mean delamination rate of inhibitor free polyaniline capsules decorated with gold nanoparticles (AuNPs@PAni) applied directly onto pretreated zinc is 330 ($\pm$ 20) $\mu m\ h^{-1}$ This value serves as a reference for the trigger signal spreading velocity, which can be accelerated by application of a polypyrrole layer (Figure 5b).

As an example, the delamination profile corresponding to a zinc substrate covered with a 1.2 μm thick PPy layer is shown in Figure 5c. The delamination profile shows a very homogenously proceeding delamination front with a rate of 380 ($\pm$ 5) $\mu m\ h^{-1}$. Due to the preferential incorporation of small cations (e.g. potassium or sodium cations which are typically present in deicing salt or sea spray) during prolonged reduction, the PPy layer provides no self-healing capability for larger defects, since the counter-anions (inhibitor) will not be released from the PPy layer. The corresponding potential at the defect site matches the free corrosion potential of zinc ($E_{corr,Zn}(pH = 7) \approx -750$ mV vs SHE) throughout the experiment, proving that the PPy layer itself does not provide protection to the macroscopic defect site (Figure 5d), as already found in other studies.[42] Hence, with respect to self-healing of macroscopic defects in such smart corrosion protection coatings it is important to focus on the release and transport of anodic inhibitors from the capsules.

In the next step, self-healing coatings with accelerated trigger signal spreading were prepared as displayed schematically in Figure 6a. Here, additional polyaniline capsules containing the inhibitor 3-nitrosalicylic acid (PAni(3-NisA)) were added in equivalent amounts for every experiment onto the polypyrrole layer. The trigger signal spreading velocity is tuned via the thickness of the polypyrrole layer as demonstrated before. The interplay between the trigger signal spreading velocity and the amount of released inhibitors from PAni(3-NisA) capsules is presented in Figure 6b. The results confirm that the release of inhibitors from the capsules, reflected by the maximum anodic shift at the defect site ΔE_{max}, increases with increasing delamination/reduction rate. The reference system without tuned trigger signal spreading velocity, which is polyaniline capsules decorated with gold nanoparticles containing the corrosion inhibitor 3-nitrosalicylic acid (AuNPs@PAni(3-NisA)) applied directly onto zinc (data at x-axis = 0), generates a ΔE_{max} of 340 mV at a delamination rate of 290 ($\pm$ 40) $\mu m\ h^{-1}$. The potential at the defect site for this reference system is shown in Figure 6c.

The delamination profile in Figure 6d shows the acceleration of the delamination rate to 980 ($\pm$ 50) $\mu m\ h^{-1}$ by the use of an intermediate PPy layer (thickness 2.9 μm), which triggers an increased release of inhibitors as reflected by the ΔE_{max} of 670 mV at the defect (Figure 6e). The potential at the delaminated/reduced interface of the corresponding delamination profile starts to shift to more noble values stepwise after about 7 h. This time corresponds to the time at which the potential at the defect turned passive ($E > -400$ mV vs SHE), implying that after passivation of the defect site the reduced ICP in the coating is re-oxidized by the atmosphere and thus polarizes the zinc|PPy interface after $\sim$2 days finally to a constant value of approx. 200 mV vs SHE (green solid line in delamination profile). The underlying mechanism by which the intermediate polypyrrole layer increases the release rate of inhibitors from the PAni(3-NisA) capsules is explained in the following (Figure 7): The electrodeposited polypyrrole (PPy) layer is doped with 3-nitro salicylate counter anions ($3\text{-}NisA^-$). Electrochemical reduction of the bipolaron states within the PPy polymer backbone occurs as a result of the decrease of electrode potential associated with zinc corrosion at the defect site. Charge neutrality is then maintained either by expulsion of counter anions (3-NisA) from PPy (Equation 1) or by migration of cations into PPy (Equation 2):[49,50]

$$PPy^{+}3NisA^{-} + e^{-} \rightarrow Ppy^{0} + 3NisA^{-} \quad [1]$$

$$PPy^{+}3NisA^{-} + e^{-} + K^{+} \rightarrow Ppy^{0}3NisA^{-}K^{+} \quad [2]$$

The high mobility of small cations (K^+) at the defect sites means that cation incorporation will be the predominant reaction and the expulsion of the rather large counter anions from PPy is not expected to be significant.[42] This was also proven to be true for the system (PPy/3-NisA) used in this work as no shift of the electrode potential at the defect site to more positive values was observed upon reduction of the connected PPy/3-NisA layer. During prolonged corrosion driven reduction of PPy, a steadily increasing amount of 3-NisA counter anions will be taken up into the ICP matrix, i.e. remain immobile, leading to steadily increasing cation incorporation and thus to a cation-selective behavior.[42,51] This eventually leads to a very fast hopping-transport of small cations and thus in the presence of large defects to a very fast coating failure.[51] Because of this, continuous layers of ICP should not be used alone in coatings for corrosion protection. Nevertheless, a continuous layer of PPy is applied here, as the fast cation transport also results in an accelerated reduction rate of PAni(3-NisA) capsules in contact with PPy due to galvanic coupling. In other words, the rate limiting step for the electrochemical reduction of PAni(3-NisA) capsules has been accelerated. Accordingly, the subsequent release of inhibitors from PAni(3-NisA) capsules significantly increases, which is reflected by the much greater shift of electrode potential at the defect site (compare Figures 6a and 6c). After passivation of the defect site, the reduction current reduces significantly so that the polypyrrole layer and the PAni(3-NisA) capsules get re-oxidized by the atmosphere. With that step, the release of inhibitors from the PAni(3-NisA) capsules stops since the capsules shell

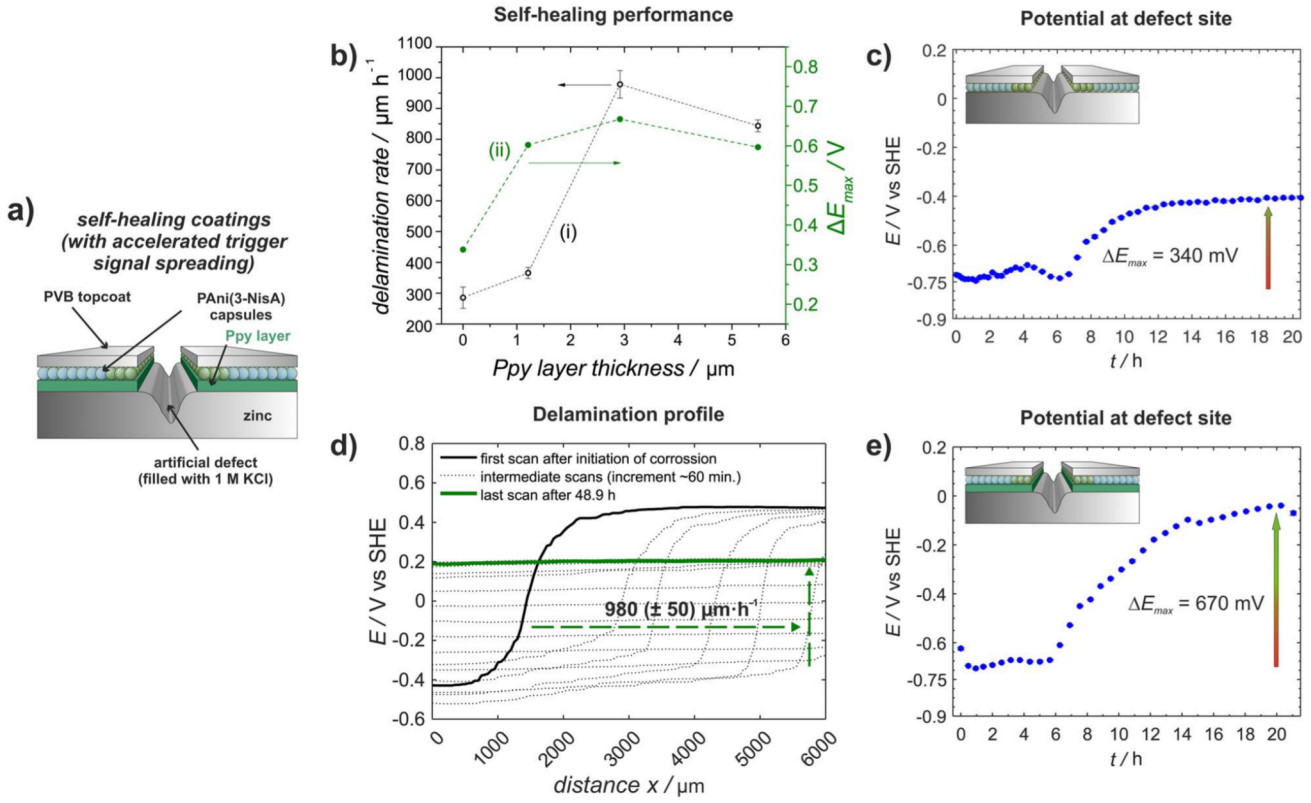

Figure 6. a) Scheme of self-healing coatings based on PPy layer combined with redox-responsive capsules filled with inhibitor. b) Delamination rate, i.e. the trigger signal spreading velocity (i), tuned as a function of PPy layer thickness, and the corresponding release of inhibitors (as reflected by the maximum shift to more noble potentials at the defect site ΔE_{max} (ii)). c) Electrode potential at the defect site for the case of AuNPs@PAni(3-NisA) capsules applied directly onto zinc (reference system). d) Delamination profile for self-healing sample with accelerated trigger signal spreading velocity (Zn/PPy(2.9µm)/PAni(3-NisA)/PVB) and e) the corresponding electrode potential at the defect site.

turns again into the impermeable oxidized state, and the Zn|PPy interface gets re-passivated as well. As passivation of the defect site alone might not be sufficient for initiating passivation of the delaminated interface, this might also indicate the presence of released inhibitors at the interface.[47]

In Figure 8 the long-term stability of the presented self-healing coatings is evaluated. Here, polypyrrole layers with a thickness of about 1.2 µm were electro-deposited onto zinc, polyaniline capsules containing the inhibitor 3-nitrosalicylic acid were deposited and PVB was used as a top-coat. The samples were stored for the denoted

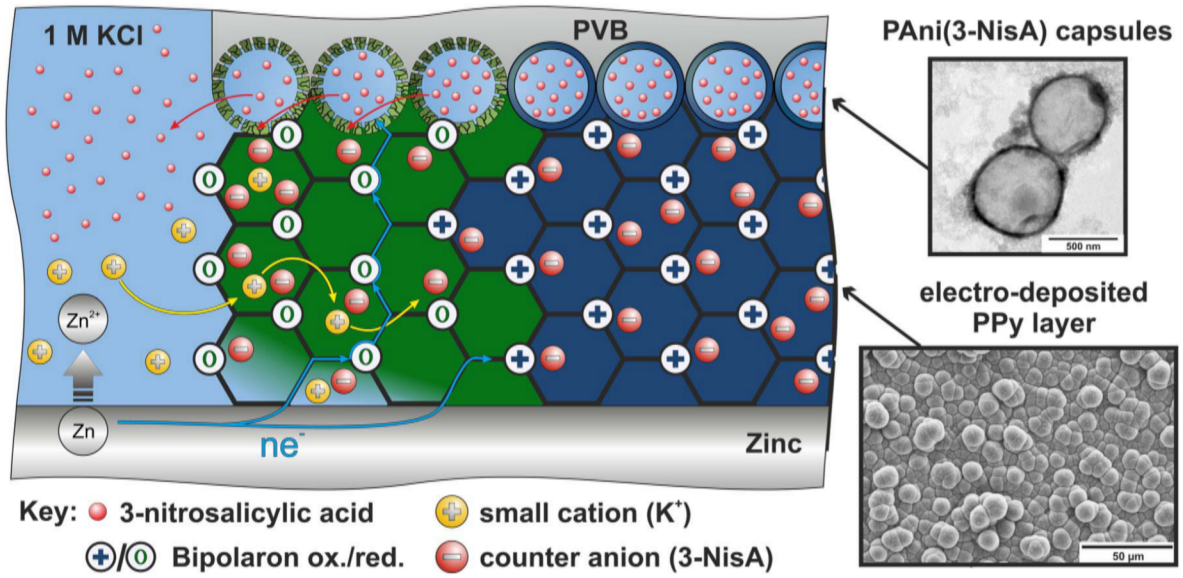

Figure 7. Schematic illustration of the mechanism by which the intermediate polypyrrole layer (top-view SEM image bottom right) accelerates the release rate of corrosion inhibitors from the PAni(3-NisA) capsules (TEM image top right). Explained in more detail in the text.

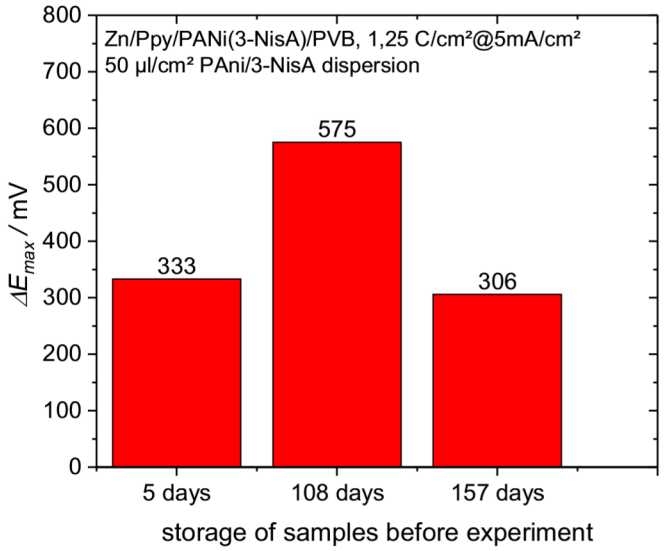

Figure 8. Evaluation of the long-term stability of self-healing samples using a scanning Kelvin probe. For each sample the maximum shift of the electrode potential measured at the defect site to more noble values are plotted.

time periods (up to 5 months) under ambient conditions. After the respective time periods, corrosion tests were conducted on the samples as described in the experimental section. The results show that the activity remains after storage of the samples for a period up to 5 months, without any indication of uncontrolled release during storage or change of mechanisms leading to passivation.

Improving the addressability of capsules far away from the metal|coating interface.—The addressability of PAni(3-NisA) capsules is usually limited to those that are in direct contact with a metal surface or a suitable conductive substrate.[35] This is due to the significantly lowered conductivity of conducting polymer in its reduced state.[52] The polyaniline shell of the capsules is rather thin, approx. 50 nm, which ensures a ready release of inhibitors.[33] However, at the same time this feature comprises the risk that capsules located farther away from the metal surface can no longer be addressed electrochemically, because the fully reduced shell of capsules underneath is not sufficiently conductive to transport the signal. Hence, it is not possible to increase the amount of releasable inhibitors simply by increasing the amount of deposited capsules.

However, it is possible to realize the electro-polymerization of PPy onto a pre-deposited layer of capsules, thus embedding them within PPy (Figure 9a). This is possible since the acidic pH and

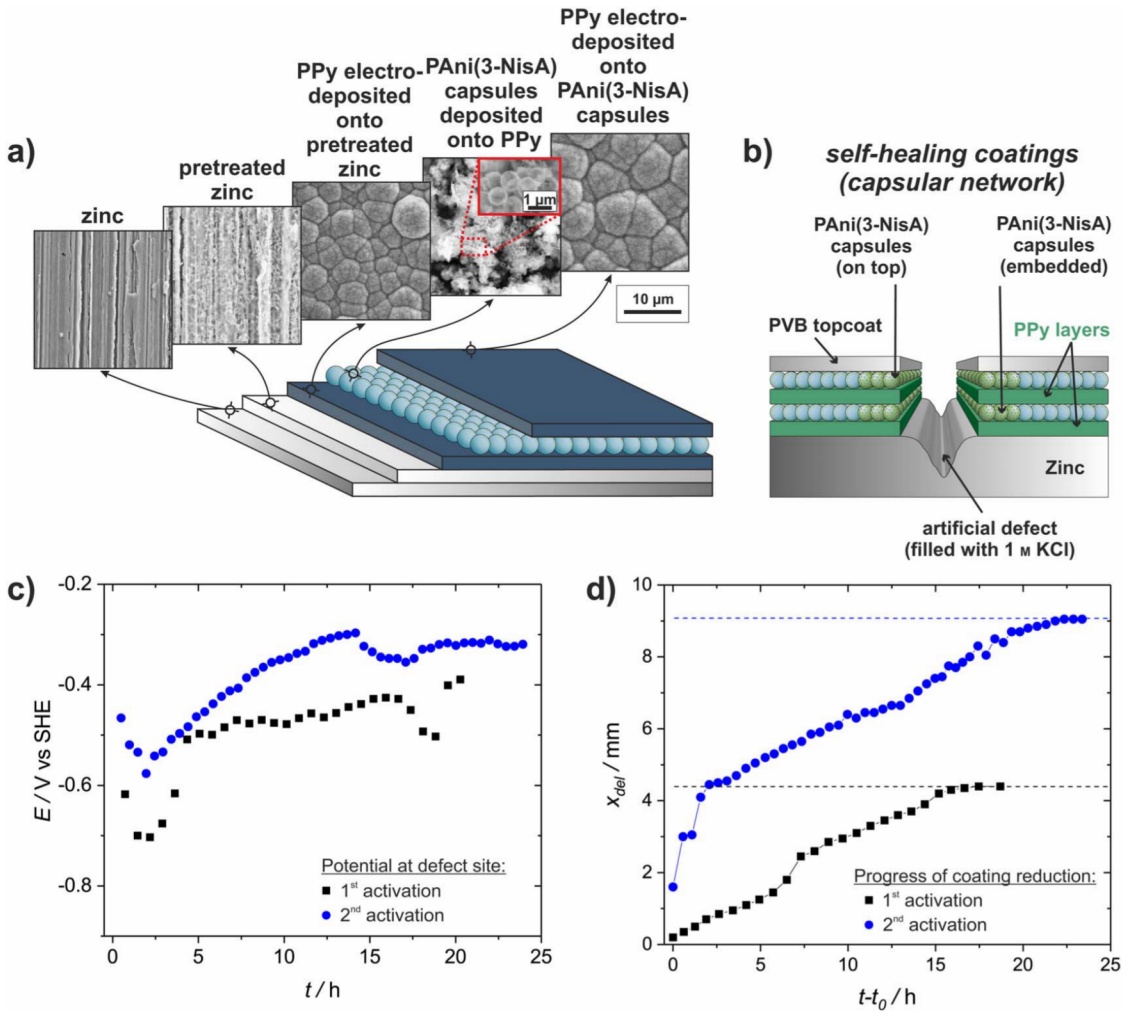

Figure 9. Increase addressability of capsules – embedding of capsules within the coating. a. coating structure of capsules embedded within PPy: the SEM micrographs show the different stages of coating preparation from left to right in plane-view. b. corresponding scheme of self-healing coatings with increased capsules loading that enables electrochemical addressability of capsules located far away from the metal surface. c. potential at defect site and d. progress of delamination (reduction) front during corrosion experiments of self-healing coating with embedded capsules: evidence of multiple self-healing and faster onset of passivation.

anodic potentials prevailing during the electro-polymerization of PPy preserve the structure of PAni capsules.[53]

Using this technique repetitively, it is possible to overcome the limitation in addressability of PAni(3-NisA) capsules vertically within the coating. The thickness of the PAni(3-NisA) capsules layer embedded within the PPy layer is kept within approx. 1.9 ($\pm$ 0.5) µm, which is rather small compared to the mean diameter of PPy aggregates (see cauliflower structure of PPy in Figure 9a) and hence, the PPy layer should provide effective conducting pathways through the capsules layer. This results in electrochemically addressable capsules, which can be located even far away from the metal surface, because these are connected via the PPy matrix. This also enables an unconstrained combination of redox-responsive containers carrying e.g. different corrosion inhibitors or other substances, such as monomer, that could further extend the functionality of the coating.

It was checked that thin layers of PAni(3-NisA) capsules, which are embedded within PPy, are still addressable and that the necessary mobility of released inhibitors within this coating is still provided. To increase the overall loading with addressable capsules, several layers of capsules can be embedded within PPy in addition to the one added on top (Figure 9b). Such self-healing coatings show faster onset of passivation at the defect site (Figure 9c) as more capsules are activated simultaneously at a certain distance from the defect. The electrode potential at the defect site starts to shift to more positive values already after ~2.3 hours; for comparison it takes about 6 hours when PAni(3-NisA) capsules are applied as a single layer onto PPy or directly onto zinc. This was found within this study and in previous publications as well.[33] The corresponding progress of delamination front stopped after approx. 16 hours at a distance of ~4200 µm. The position of the delamination front x_{del} is plotted as a function of elapsed time t-t_0 in Figure 9d.

Even multiple self-healing of macroscopic defects (with increasing size) at the same position is achieved: after self-healing of the first defect the experiment was repeated with fresh electrolyte and a new defect at the same position. During this 2nd activation, the potential at the defect site dropped from approx. −450 mV vs. SHE to −600 mV vs. SHE within the first 2.5 hours of the experiment, which was again followed by an increase in electrode potential (2nd activation in Figure 9c). The higher electrode potential at the beginning of the experiment as compared to the one observed for the first activation, might be due to remaining inhibitor released before in the area of the defect and the surrounding coating. It was also observed that the electrode potential increases slower as compared to the first activation, which could reflect a loss in stored inhibitor within the PAni(3-NisA) capsules and the increasing distance over which the released inhibitors have to be transported toward the defect site. It can also be assumed that the fraction of released inhibitor that effectively reaches the defect site decreases with increasing distance to the defect site, as the transportation of released inhibitor is a diffusion-controlled process without a preferred direction. The delamination front of the 2nd activation rapidly reaches the position at which the delamination front of the first activation stopped. This can be due to a number of reasons. For example, it can be due to remaining electrolyte which was taken up by reduced PPy during the first activation period or a imperfectly restored interface. Note, the sample was not completely dried between both activations, just the scratch was renewed, and the electrolyte exchanged. However, this second even somewhat larger defect was also successfully passivated, as the potential at the defect site reached after ~12.5 hours a constant value of ~−300 mV vs SHE (which was monitored for approx. 1 day) and the progress of delamination stopped after ~22 hours at a position of approx. 9 mm.

Conclusions

This work demonstrates the interplay of the velocity of trigger signal spreading and the self-healing performance of smart coatings. On the basis of a practically relevant example, it was shown how the velocity of trigger signal spreading (laterally and vertically within the active coating) can be improved, leading to superior self-healing performance. This was achieved by combining a layer of ICP with redox responsive capsules carrying active agents. More specifically, this continuous layer of ICP accelerates the spreading of the corrosion induced decrease of the electrode potential, which is conventionally associated with extremely weak coating performance, but here it serves as a tunable trigger signal. Thus, the weakness of an ICP layer can be turned into strength, while all positive aspects of ICP coatings are preserved. Those comprise an intrinsic interfacial metal|coating stability with inherent protection of weak spots within the coating, such as pinholes or cracks, the ability to restore the activated coating after healing of the local damage and the possibility to increase the addressability of containers storing active agents. The latter aspect was shown to enable a faster onset of the healing process and a multiple self-healing of macroscopic defects. This coating design can also serve as a basis for an unconstrained combination of various redox-triggered containers carrying different healing agents, since the trigger signal can be directed far away from the metal|coating interface.

In summary this work shows, that for designing trigger based smart self-healing materials it might be rewarding to leave established rules behind and follow new directions, even some that appear to be counter-intuitive at first.

Acknowledgments

M. Uebel, D. Crespy and M. Rohwerder gratefully acknowledge the financial support from DFG SPP 1568 “Design and Generic Principles of Self-Healing Materials”. M. Rabe acknowledges funding by the European Union’s Horizon 2020 research and innovation programme under the Marie Skłodowska-Curie grant Agreement No. 705857.

ORCID

Matthias Uebel https://orcid.org/0000-0002-7825-7047
Michael Rohwerder https://orcid.org/0000-0002-2466-3963

References

1. A. E. Hughes, I. S. Cole, T. H. Muster, and R. J. Varley, *Npg Asia Mater*, **2**(4), 143 (2010).
2. N. G. T. G. H. Koch, O. Moghissi, J. H. Payer, and J. Varney, NACE International, Houston, TX 2016.
3. M. Stratmann, *Corrosion*, **61**(12), 1115 (2005).
4. O. Gharbi, S. Thomas, C. Smith, and N. Birbilis, *npj Materials Degradation*, **2**(1), 12 (2018).
5. S. A. Katz and H. Salem, *J. Appl Toxicol*, **13**(3), 217 (1993).
6. J. Sinko, *Prog Org Coat*, **42**(3–4), 267 (2001).
7. S. R. White, N. R. Sottos, P. H. Geubelle, J. S. Moore, M. R. Kessler, S. R. Sriram, E. N. Brown, and S. Viswanathan, *Nature*, **409**(6822), 794 (2001).
8. I. S. Cole, *Woodh Publ Ser Metal*, (64), 29 (2014).
9. M. F. Montemor, *Surf Coat Tech*, **258**, 17 (2014).
10. M. L. Zheludkevich and A. E. Hughes, *Springer Ser Mater S*, **233**, 157 (2016).
11. D. Crespy, K. Landfester, J. Fickert, and M. Rohwerder, *Self-Healing Materials*, **273**, 219 (2016).
12. S. J. Garcia, H. R. Fischer, P. A. White, J. Mardel, Y. Gonzalez-Garcia, J. M. C. Mol, and A. E. Hughes, *Prog Org Coat*, **70**(2–3), 142 (2011).
13. S. H. Cho, H. M. Andersson, S. R. White, N. R. Sottos, and P. V. Braun, *Advanced Materials*, **18**(8), 997-+ (2006).
14. W. Furbeth and M. Stratmann, *Prog Org Coat*, **39**(1), 23 (2000).
15. D. V. Andreeva, E. V. Skorb, and D. G. Shchukin, *Acs Appl Mater Inter*, **2**(7), 1954 (2010).
16. D. G. Shchukin, S. V. Lamaka, K. A. Yasakau, M. L. Zheludkevich, M. G. S. Ferreira, and H. Mohwald, *J. Phys Chem C*, **112**(4), 958 (2008).
17. D. Borisova, D. Akcakayiran, M. Schenderlein, H. Mohwald, and D. G. Shchukin, *Adv Funct Mater*, **23** (30), 3799 (2013).
18. M. Kendig and M. Hon, *Corrosion*, **60**(11), 1024 (2004).
19. G. Williams, S. Geary, and H. N. McMurray, *Corros Sci*, **57**, 139 (2012).
20. H. N. McMurray and G. Williams, *Corrosion*, **60**(3), 219 (2004).
21. V. Shkirskiy, P. Keil, H. Hintze-Bruening, F. Leroux, P. Vialat, G. Lefevre, K. Ogle, and P. Volovitch, *Acs Appl Mater Inter*, **7**(45), 25180 (2015).
22. E. Alibakhshi, E. Ghasemi, M. Mandavian, and B. Ramezanzadeh, *Corros Sci*, **115**, 159 (2017).
23. V. Shkirskiy, P. Keil, H. Hintze-Bruening, F. Leroux, T. Stimpfling, D. Dragoe, K. Ogle, and P. Volovitch, *Corros Sci*, **99**, 31 (2015).
24. S. A. S. Dias, A. Marques, S. V. Lamaka, A. Simoes, T. C. Diamantino, and M. G. S. Ferreira, *Electrochim Acta*, **112**, 549 (2013).

25. T. Stimpfling, P. Vialat, H. Hintze-Bruening, P. Keil, V. Shkirskiy, P. Volovitch, K. Ogle, and F. Leroux, *Eur J. Inorg Chem*, (13–14), 2006 (2016).
26. F. Maia, J. Tedim, A. D. Lisenkov, A. N. Salak, M. L. Zheludkevich, and M. G. S. Ferreira, *Nanoscale*, **4**(4), 1287 (2012).
27. S. Jiang, L. P. Lv, K. Landfester, and D. Crespy, *Accounts Chem Res*, **49**(5), 816 (2016).
28. N. LeBozec, D. Thierry, M. Rohwerder, D. Persson, G. Luckeneder, and L. Luxem, *Corros Sci*, **74**, 379 (2013).
29. W. Furbeth and M. Stratmann, *Corros Sci*, **43**(2), 207 (2001).
30. C. Senoz and M. Rohwerder, *Electrochim Acta*, **56**(26), 9588 (2011).
31. L.-P. Lv, Y. Zhao, N. Vilbrandt, M. Gallei, A. Vimalanandan, M. Rohwerder, K. Landfester, and D. Crespy, *Journal of the American Chemical Society*, **135**(38), 14198 (2013).
32. W. Leng, S. Zhou, G. Gu, and L. Wu, *J. Colloid Interf Sci*, **369**(1), 411 (2012).
33. A. Vimalanandan, L.-P. Lv, T. H. Tran, K. Landfester, D. Crespy, and M. Rohwerder, *Advanced Materials*, **25**(48), 6980 (2013).
34. M. Rohwerder, S. Isik-Uppenkamp, and C. A. Amarnath, *Electrochim Acta*, **56**(4), 1889 (2011).
35. A. Vimalanandan, Ruhr Univeristät Bochum, Bochum, 2016.
36. A. Michalik and M. Rohwerder, *Z Phys Chem*, **219**(11), 1547 (2005).
37. B. Muller and J. Langenbucher, *Corros Sci*, **45**(2), 395 (2003).
38. M. Uebel, A. Vimalanandan, A. Laaboudi, S. Evers, M. Stratmann, D. Diesing, and M. Rohwerder, *Langmuir*, **33**(41), 10807 (2017).
39. A. Leng, H. Streckel, and M. Stratmann, *Corros Sci*, **41**(3), 547 (1999).
40. G. L. Duffitt and P. G. Pickup, *J. Chem Soc Faraday T*, **88**(10), 1417 (1992).
41. M. Rohwerder, L. Duc, and A. Michalik, *Electrochim Acta*, **54**(25), 6075 (2009).
42. G. Paliwoda-Porebska, M. Rohwerder, M. Stratmann, U. Rammelt, L. M. Duc, and W. Plieth, *J. Solid State Electr*, **10**(9), 730 (2006).
43. M. Rohwerder and M. Stratmann, *Mrs Bull*, **24**(7), 43 (1999).
44. B. Wessling, *Werkst Korros*, **47**(8), 439 (1996).
45. M. Stratmann and H. Streckel, *Corros Sci*, **30**(6–7), 681 (1990).
46. G. S. Frankel, M. Stratmann, M. Rohwerder, A. Michalik, B. Maier, J. Dora, and M. Wicinski, *Corros Sci*, **49**(4), 2021 (2007).
47. G. Williams and H. N. McMurray, *J. Electrochem Soc*, **148**(10), B377 (2001).
48. T. H. Tran, A. Vimalanandan, G. Genchev, J. Fickert, K. Landfester, D. Crespy, and M. Rohwerder, *Advanced Materials*, **27**(25), 3825 (2015).
49. K. Naoi, M. Lien, and W. H. Smyrl, *J. Electrochem Soc*, **138**(2), 440 (1991).
50. D. Chen and Q. B. Pei, *Chem Rev*, **117**(17), 11239 (2017).
51. M. Rohwerder and A. Michalik, *Electrochim Acta*, **53**(3), 1300 (2007).
52. W. W. Focke, G. E. Wnek, and Y. Wei, *J. Phys Chem-Us*, **91**(22), 5813 (1987).
53. S. C. Hobaica, *J. Polym Sci Pol Phys*, **41**(8), 807 (2003).